This is a peer-reviewed, author's accepted manuscript of the following research article: Sharif, S., Ahmad, Z., Hoskins, C., Choudhary, M. A., & Mehmood, A. (2022). Ag nanostructure morphologies and physicochemical properties dictated by the polyols used in the synthesis. *Journal of Nano Research*, *76*, 93-106. https://doi.org/10.4028/p-c41elh

The Effect of a Mixed Polyol Synthesis of Ag Nanostructures on their Structure, Morphology and Physicochemical Properties

Sadia Sharif[1], Zahoor Ahmad*[1], Clare Hoskins[2], Muhammad Aziz Choudhary[1], Arshad Mehmood[2]

[1]Department of Chemistry, Mirpur University of Science and Technology (MUST), 10250, Mirpur AJK, Pakistan.

[2]Department of Pure and Applied Chemistry, University of Strathclyde, Glasgow, G1 1RD, UK

[3]Material Science and Engineering Division, National Institute of Laser and Optronics (NILOP), PIEAS, Nilore, Islamabad.

*zahoor.chem@must.edu.pk

Graphical abstract

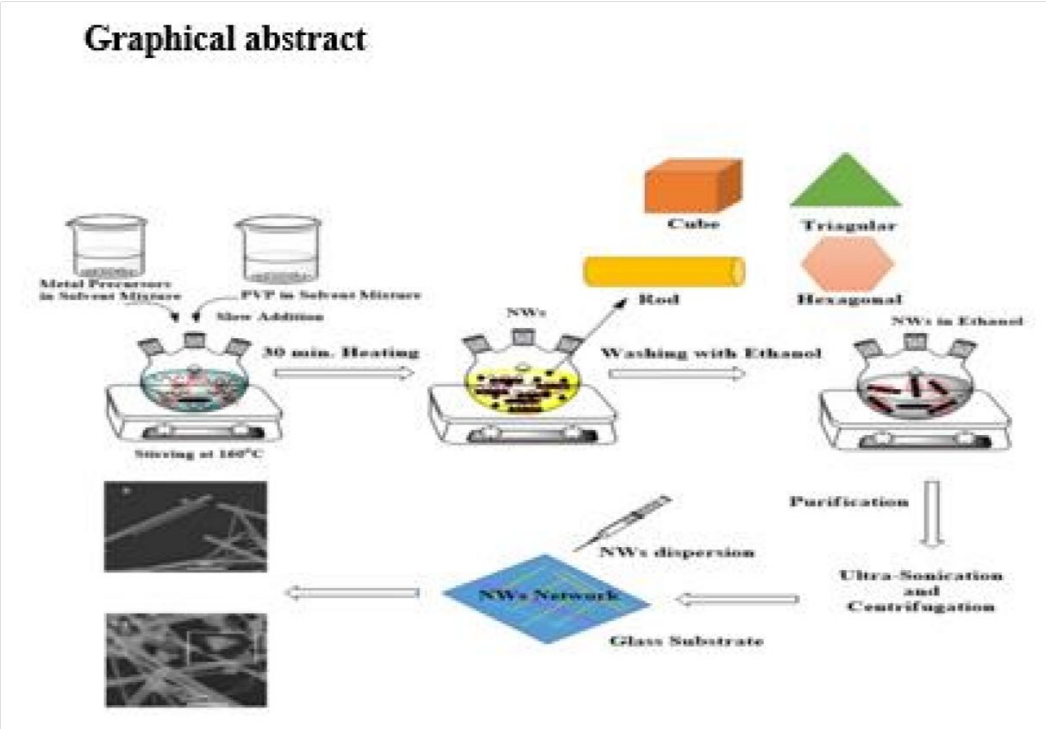

Abstract: The mixing of ethylene glycol (EG) with diethylene glycol (DEG) has been studied to analyse the effect of viscosity rise of solvent on the Ag nanostructures and their morphologies. The rise of viscosity has been adjusted by increasing the molar ratio of DEG to EG under optimized conditions of temperature and capping agent- poly (vinylpyrrolidone) (PVP). It has been seen that increasing the proportion of DEG resulted increasing the viscosity of solution and thus decreased the diameter of nanowires. The production of quantum nanowires has further become possible during reaction. The synthesized material was characterized using UV−Vis spectroscopy, SEM, EDX, XRD, PL and DSC. Surface Plasmon resonance and luminescence was determined using UV−Vis spectroscopy and PL spectroscopy. The data showed that Ag nanowires have a strong absorption band at 356 nm and 401 nm which can be attributed to the transverse and longitudinal surface Plasmon resonance. The XRD results indicated that the prepared product is made of pure Ag with face centred cubic structure, and the DSC analysis demonstrated the presence of amorphous domain within metal nanostructures. Finally, temperature fluctuations have caused the formation of nanoparticle of different shapes and sizes which bears the synthetic mechanistic insights.

1. Introduction

1-D silver nanowires (Ag NWs) have been particularly investigated recently, due to their excellent optoelectronic, mechanical, thermal and catalytic properties [1-3]. These have been used as prime interconnects in the integrated circuit units of many nanodevices. The NWs can be tuned to control the transfer of electron at a single electron level by controlling their diameter and applied voltage. Therefore, different methods for synthesis of Ag NWs have been developed, like hydrothermal, electrochemical, liquid-phase synthesis, solvothermal co-reduction method, ultraviolet irradiation, thermal reduction, vacuum vapour deposition and polyol process [4-6]. These are aimed to regulate their morphologies, structures and properties.

The polyol process mainly employs ethylene glycol (EG) as a reducing agent for the synthesis of Ag NWs; it is also a suitable solvent for $AgNO_3$ and PVP, due to its high polarity and dielectric constant [7-9]. Usually, an oxygen free environment is preferred to avoid oxidation of nanostructure [10-11]. Interestingly, polyol process has been shown to be the most promising methods, mainly because the preheating required results in an aqueous/oxygen free system which can avoid surface oxidation [12]. Its high viscosity, polarity and dielectric constant resist against agglomeration, and further help to tailor the pristine Ag nanostructures [13]. Changchao Jia and co- workers synthesized Ag NWs and NPs using glycerol and EG as solvents where large number of Ag nanoparticles (NPs) and few Ag NWs were observed [14]. The production of NWs has been improved, when optimized quantities of DEG, TEG and glycerol were mixed with EG.

Additionally, a sodium bromide (NaBr) solution has been used in the polyol process which further improved the production of Ag NWs [15]. Such outcomes have been suggested to be a result of the increase in solution viscosity,

which decreased the Ag^+ migration rate onto a growing nanostructure. It further resulted in a decrease in the diameter and an increase in the length of the Ag NWs [16-17].

Polyol being a versatile method is also very helpful in controlling the length and diameter of Ag nanostructures and tuning its properties. In this study, we focus to further enrich polyol process by mixing of EG and DEG with many proportional ratios and gradually increased the viscosity of each solution, while maintaining all other parameters constant. This method allowed us to synthesize Ag NWs possessing a high aspect ratio with tuneable diameter. We also observed the particles formation of different shapes and sizes, which is advantageous in allowing us to understand the mechanistic growth of Ag NWs under varying solvent conditions. The produced NWs have been investigated for their optical properties, as well as the properties of their amorphous domain within as designed NSs, which can be further related to elaborate the quantum confinement effect and quantum freedom effect, where ψ function can freely spread.

2. Experimental

2.1. Materials

All chemicals were purchased from commercial sources. Polyvinyl pyrrolidone (PVP, Mw ≈ 90,000) was purchased from Sigma Aldrich. Diethylene glycol (DEG) and sodium chloride (NaCl, ≥ 99.0%) were purchased from the Shanghai Chemical Reagent Company. Similarly, ethylene glycol (EG, 99%) and sodium nitrate ($AgNO_3$) were purchased from Duksan Pure Chemicals, absolute ethanol from Merck and acetone from Ridel-de-Haen.

2.2. Synthesis of Ag Nanowires

Ag NWs were prepared using a polyol reduction method, where both EG and DEG have been used. In a typical synthesis, 10 ml EG was pre-heated for 30 min at 160 ^{0}C. Then, a 0.01M NaCl solution (60 µl) was added and subsequently 5 ml of 0.17M $AgNO_3$ & 5 ml of 0.18M PVP solutions prepared in EG, EG-DEG mixture and DEG were added. These solutions were added simultaneously to preheated pure EG following an injection rate 0.2 ml/min. Six samples have been prepared which are designated as E_1D_0, E_2D_1, E_3D_2, E_4D_3, E_5D_4 and E_0D_5 due to the EG:DEG ratio; 10:0, 8:2, 6:4, 4:6, 2:8 and 0:10, respectively. The reaction mixtures turned blue at very initial stage, however as the addition proceeded, the colour changed from yellow green, pale yellow and finally grey. The reaction was allowed to continue for one hour.

As synthesized Ag NWs and other nanostructures were purified using sonication and centrifugation in acetone and ethanol. For this, acetone (almost double volume) was added to reaction mixture and centrifuged at 3000 rpm for 15 min. The Ag NWs were washed several times with ethanol until the supernatant became clear. The Ag NWs were dispersed in ethanol before characterization.

The composition of each sample with designation is given in a Table 1.

Table. 1 Designation and compositions of the samples

Sample:	EG /mL	DEG /mL	AgNO3 /g	NaCl /g	PVP /g
E_1D_0	10	0	0.143	0.008	0.09
E_2D_1	8	2	0.143	0.008	0.09
E_3D_2	6	4	0.143	0.008	0.09
E_4D_3	4	6	0.143	0.008	0.09
E_5D_4	2	8	0.143	0.008	0.09
E_0D_5	0	10	0.143	0.008	0.09

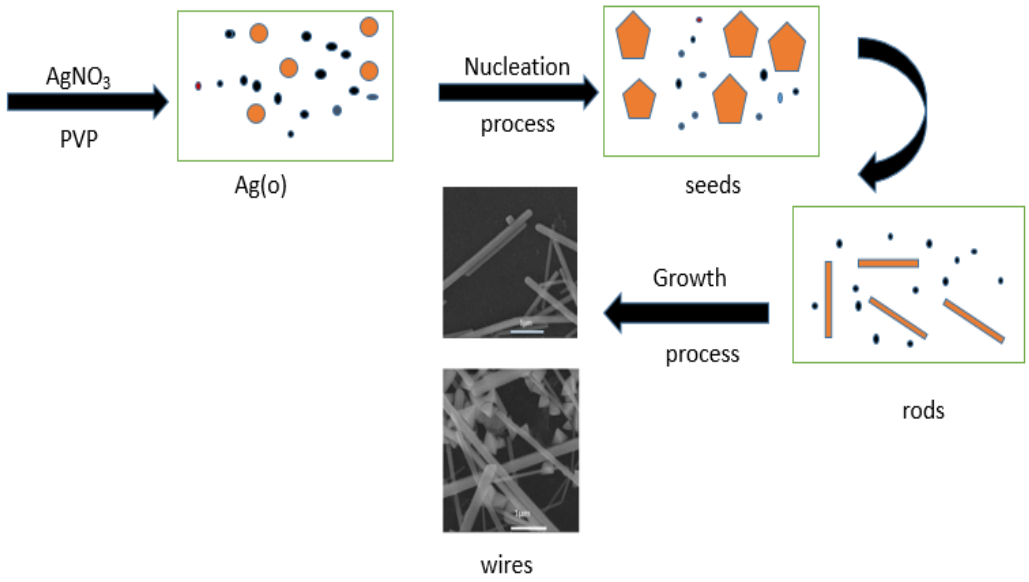

Scheme 1. Mechanism of Silver Nanowires

2.3. Characterization

The samples were characterized using a SHIMADZU 1800 UV-Vis spectrophotometer. The crystallinity and phases of the Ag NWs were characterized using an X-ray diffractometer (Bruker's D8-discoverer). The chemical

composition and morphological observations were determined using a TESCAN MIRA3 XMU scanning electron microscope. Fluorescence of each sample was analysed using a SHIMADZU RF-6000 Spectrophotoflourometer. Thermal properties for investigating amorphous domain were studied by employing PerkinElmer Differential Scanning Calorimeter 6000.

3. Results and Discussion

3.1 SEM and EDX characterization

Firstly, the effect of DEG proportion in EG on morphology of the Ag NWs was investigated. DEG has higher viscosity (30 mPa·s at 25 ºC) than EG (17 mPa: at 25 ºC) due to having more hydrogen bonding. This resulted an increase in the viscosity of the mixed solvent, which appeared to slow down the migration of Ag^+ onto the growing nanostructure, making them thermodynamically favourable [18]. The increased viscosity affected in diameter, with Ag NWs possessing decreased diameters being observed; thereby increasing the length and aspect ratio of the Ag NWs [19-21]. Furthermore, the appearance of new structures formed appeared in different forms including tetrahedral, cubic, triangular, hexagonal, rod like, capsule and rhombic shaped particles which was solvent mixture dependent, Figure 1(a-f). According to the Fig 1a the nanostructures produced from the E_1D_O solvent mix, where the dominant product is Ag NWs which possess a diameter between 70-80 nm and length in the μm scale. Such observations are quite in accordance with reported data [22]. However, as the proportion of DEG is increased, Ag NWs with small diameter were observed, along with the presence of NPs of differing shape, dependent on the DEG constituent. The results of these samples are expressed in Figure 1(b-f), showing the images for samples E_2D_1, E_3D_2, E_4D_3, E_5D_4, E_0D_5 respectively. The SEM image of E_2D_1 given in Figure 1b (1&2) shows the presence of Ag NWs with a diameter of 60 -70 nm, as well as ultrathin Ag NWs with diameters of approximately 35 nm also present. Such Ag NWs were not observed in Figure1a. These quantum wires can control conduction of even a few electrons. Moreover, the shape observed in this sample is tetrahedral particles which is being highlighted in the inset of Figure b1. While in Figure1 (c) the diameter of Ag NWs of sample E_3D_2 is 55-60 nm with ultrathin Ag NWs possessing diameters of approximately 30 nm present along with the large hexagonal and cubic NPs present as a particular shape. Similarly, Figure1 (d) shows that diameter of the Ag NWs formed from E_4D_3 are observed to be 55-60 nm, with the presence of ultrathin wires around 30 nm diameter, along with NPs with geometry tetrahedral, triangular and cubic shapes. Likewise, Figure1 (e) depicted that the diameter of Ag NWs of sample E_5D_4 is 50-60 nm similar to the E_3D_2 sample with ultrathin wire diameter 30 nm as well as the presence of cubic, tetrahedral and hexagonal nanoparticles, along with rod like particles. Figure 1(f) shows the diameter of Ag NWs formed from the E_0D_5 solvent mix, which is 50-55 nm and similarly, along with ultrathin NWs bearing diameter 30 nm. It also displayed the formation of tetrahedral, capsule, cubic nanostructures, with additional rhombic shaped particles. On reviewing the formation NPs, it was observed that the formation of tetrahedral is particular to the E_2D_1 sample, hexagonal and cubic in E_3D_2, triangular in E_4D_3, rod like in E_5D_4, and finally the capsule and rhombic in E_5D_4. Such hierarchical formation leads to the foundational materials such as triangular, rhombic, capsule and rod like NPs. These formations are prerequisite for anisotropic growth that develop into Ag NWs and quantum Ag NWs. These observations suggested clear mechanistic evidence of nano intermediates for

the complete design of Ag NWs. The observed order of the transformation of shapes is; rhombic-triangular-hexagonal-tetrahedral-NWs.

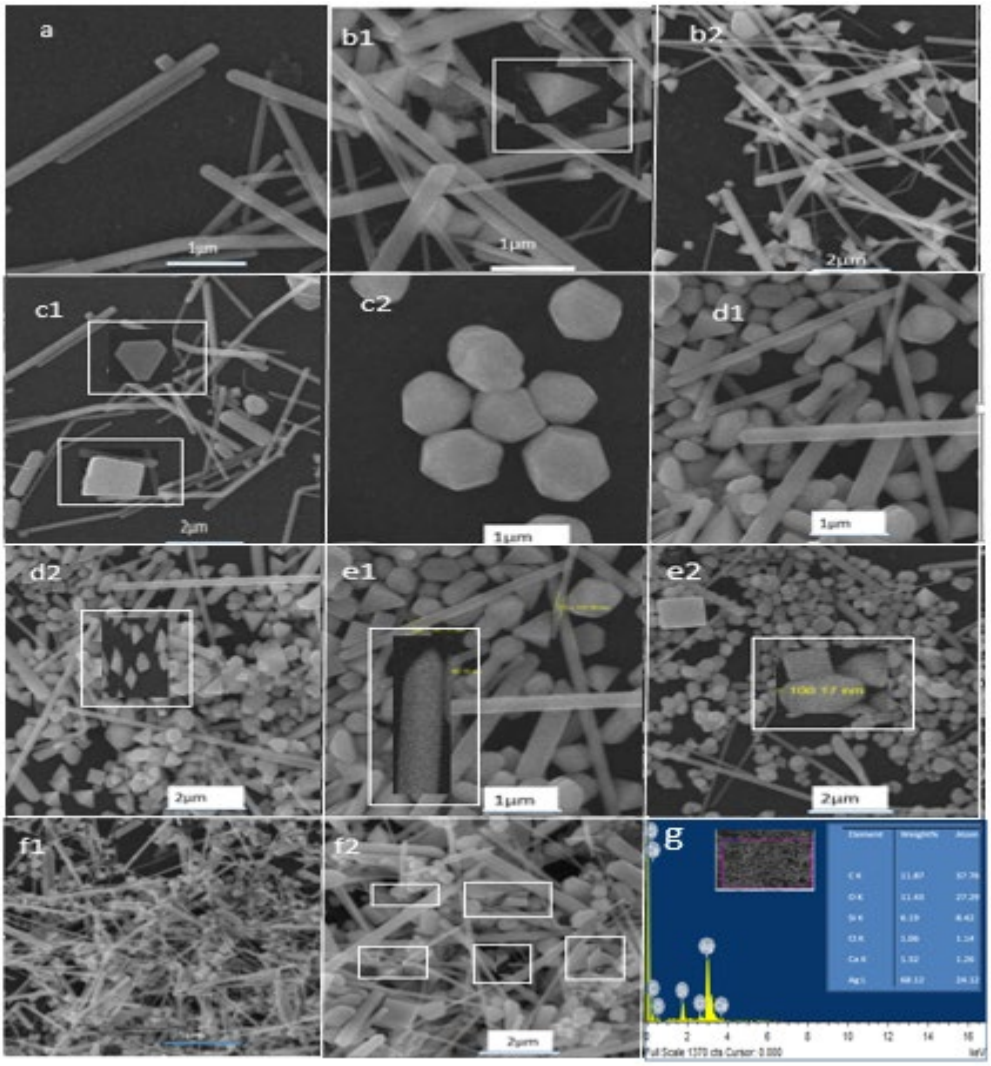

Figure 1. SEM micrograph displays the formation of Nanostructures produced from (a)E_1D_0, (b)E_2D_1, (c)E_3D_2, (d)E_4D_3, (e) (E_5D_4, (f)E_0D_5 and (g) represents the EDX pattern of Ag NWs

EDX characterization of Ag NWs on a silicon substrate are shown in Figure 1(g). The data shows that the samples are composed of almost pure silver with only a few other elements detected.

3.2 X-ray Diffraction Analysis (XRD)

X-ray diffraction was used to study the degree of crystallinity of the Ag NWs in Fig 2(a-e). According to Figure 2(a), four distinct diffraction peaks at 2θ: 38.13°, 44.4°, 64.4° and 77.4° have been assigned the plane: (111), (200), (220), (311) respectively. The diffraction peaks are indexed to the face centred cubic (fcc) phase of silver,

which agrees to other reported data [23-24]. Figure 2(b) shows additional peaks observed at 2θ: 33.46° with plane (122), and another two peaks at 45° and 51° due to the hexagonal phase of the silver related to planes (103) and (104). However, the (111), (200), (220) and (311) planes appeared at 2θ in Figure 2(b) are similar to Figure 2(a). In Figure 2(c), dominant peak located at diffraction angle 38.20° (111). Figure 3(d) shows highest peak located at diffraction angle 38.10° (111) with some additional peaks also present. While Figure 2 (e) further shows anisotropic behaviour, however at 20° there is a peak related to PVP, which is present due to its affinity with particles in the sample. Usually, the binding of nanoparticles with polymer is more, so it can be interpreted that sufficient existence of polymer is there, which appeared in XRD. The remaining four distinct diffraction peaks of Ag in Figure 2 (e) are like peaks in Figure 2(a). The role of capping agent to develop Ag NWs at high enthalpy is related to its preferential binding ability with (100) lattice phase of crystal surface and allowing "Ag" deposition at (111) lattice planes. Thus, suppressing the one phase and allowing the growth at other thermodynamically stable phase result the production of Ag NWs [25-26].

According to the experimental data, the lattice spacing of the synthesized silver nanowires for samples (E_2D_1, E_3D_2, E_4D_3, E_5D4, E_0D_5) is determined to be 2.35Å, 1.82 Å, 2.36 Å, 2.35 Å, 2.37 Å. The silver nanowire location of (111) is preferred because, in the FCC lattice, the atom density of the (111) crystal surface is 90.7%, which is considerably higher than that of the (100) crystal surface. The crystallite size is calculated by using Scherer Equation 1:

$$D = K\lambda / \beta\cos\theta \qquad (1)$$

The average crystallite size calculated from most dominant peak $2\theta = 38^0$ in the XRD pattern was found to 5.1 nm.

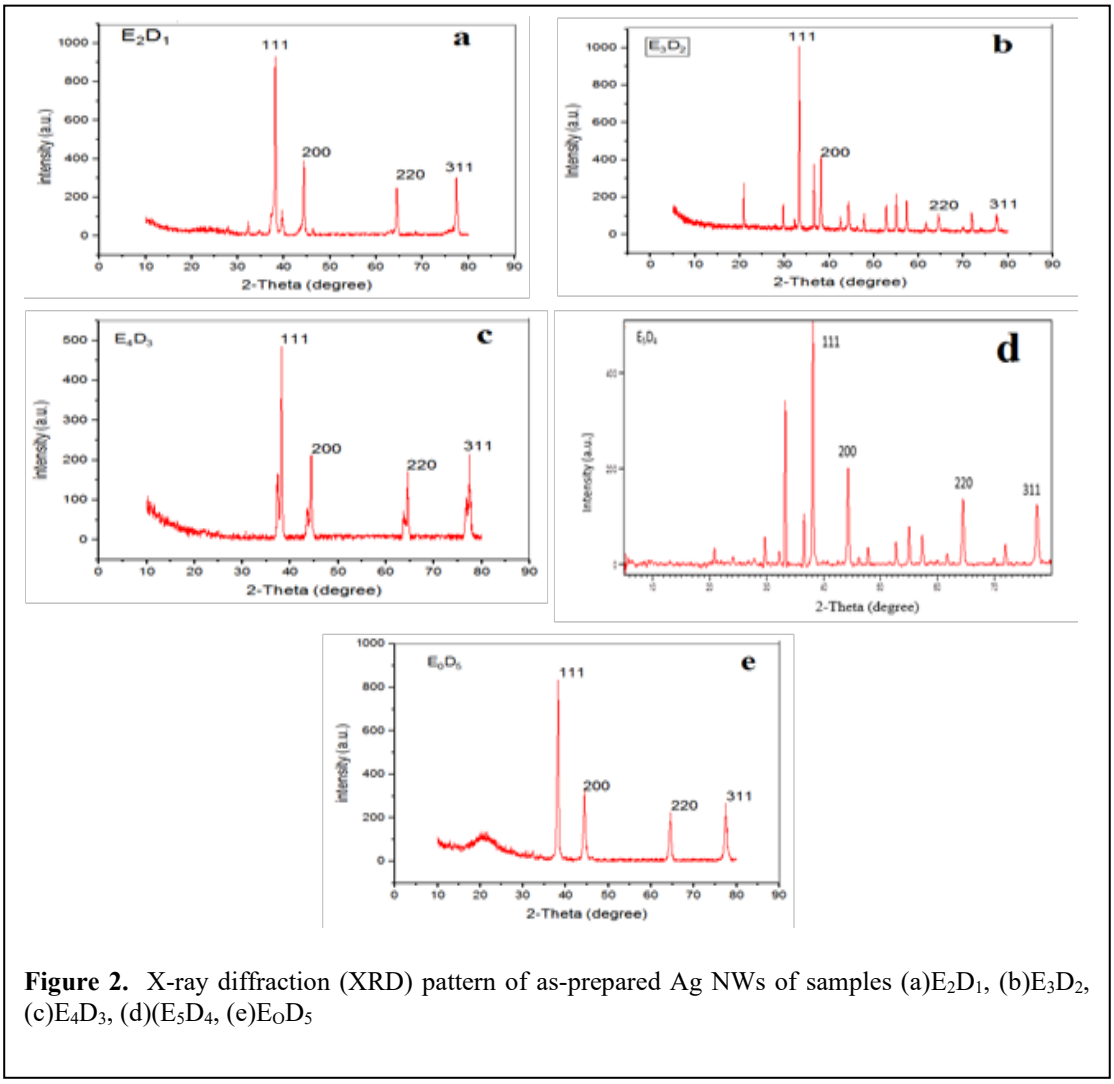

Figure 2. X-ray diffraction (XRD) pattern of as-prepared Ag NWs of samples (a)E_2D_1, (b)E_3D_2, (c)E_4D_3, (d)(E_5D_4, (e)E_OD_5

3.4 UV-**Visible spectroscopy**

Surface Plasmon resonance was determined for each sample via lambda max measurement on a UV–Vis Spectrophotometer. The morphological evolution of Ag NWs displayed in Figure 3 (a-e) shows the surface Plasmon resonance and the morphological evolution of Ag NWs. The shapes and sizes of the metal nanostructures produced varying degrees of SPR at different wavelengths [27-28]. According to the literature, the absorption peak of silver nanowires occurs between 350 nm and 380 nm [29]. For silver nanowires, this range is the transverse Plasmon resonance absorption peak. In Figure 3(a) two relatively sharp SPR peaks are observed at 356 nm and 386 nm which belong to the transverse plane of Ag NWs. The shoulder peak at 356 nm is attributed to out-of-plane quadrupole resonance and peak at 386 nm is due to out-of-plane dipole resonance of the Ag NWs. Figure 3 (b) shows a shoulder peak present at 358 nm and a broad absorption band at 428 nm which is due to the π -π* transitions. Figure 3(c) show peaks at 357 nm and 426 nm while in Figure 3(d), shoulder and broad absorption

peaks are observed at 348 nm and 413 nm. Figure 3(e) shows peaks at 357 nm and 423 nm while in Figure 3(f) the observed peaks are at 357 nm and 446 nm.

The band gap of Ag NWs is calculated using the Equation 2:

$$Eg = hc/\lambda \quad (2)$$

Where Eg is for band gap, hc are constant and λ is an absorption wavelength, the calculated band gap of Ag NWs is 2.82 eV. The existence of band gap in Ag NWs or nanostructures clearly demonstrates that ψ function of electron is restricted in nano domain, which is supported by many studies and thus allowed in micro domain for the conduction of electrons [30].

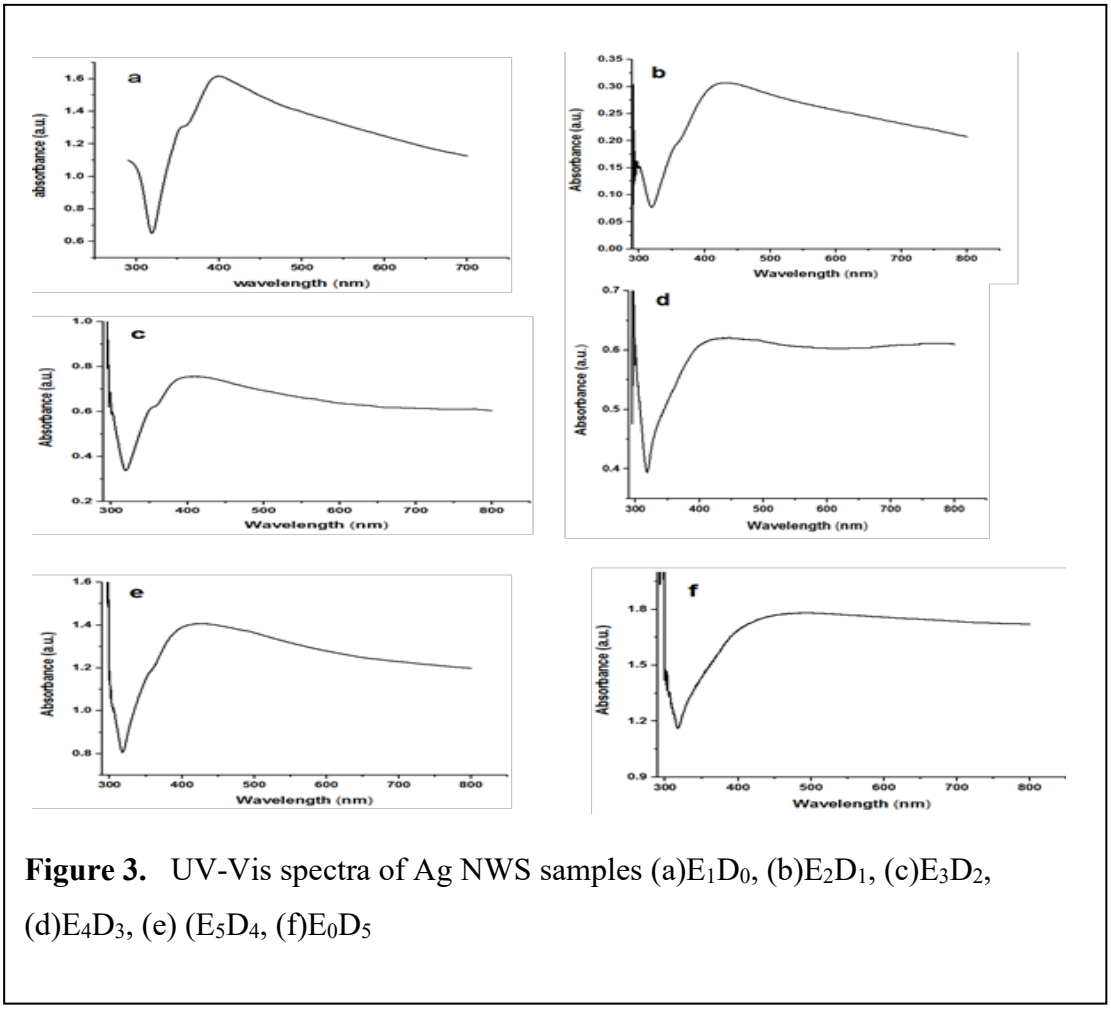

Figure 3. UV-Vis spectra of Ag NWS samples (a)E_1D_0, (b)E_2D_1, (c)E_3D_2, (d)E_4D_3, (e) (E_5D_4, (f)E_0D_5

3.5 Photoluminescence spectroscopy

The light harvesting property of the samples was investigated using Photoluminescence Spectroscopy (PL) [31]. Metal nanostructures fluorescence is not limited to single wavelength, their fluorescence is established on excitation and emission wavelengths [32]. The PL spectra of Ag NWs at different excitation wavelengths are shown in Figures 4 (a). The variations of PL emission from the Ag NWs dispersed in ethanol were recorded at the

excitation wavelengths; 354 nm, 357 nm, 356 nm, 359 nm, 367 nm for samples E_2D_1, E_3D_2, E_4D_3, E_5D_4, E_0D_5. The blue–green PL emission for every sample has been observed within range of 446 nm, 451 nm, 460 nm, 462 nm, 474 nm. In Figure 4(b) excitation wavelengths are at 400 nm, 414 nm, 416 nm, 418 nm, 440 nm. The emission bands observed in the range 480 nm, 514 nm, 517 nm, 527 nm, 531 nm and these emissions are assigned to radiative recombination of Fermi level electrons and sp- or d-band holes. Inset of Figure 4(a, b) luminescence has also been seen from the range 480 nm-531 nm. The fluorescence of Ag is more evident in sample E_4D_3 which is more intense compared to other samples. High enhancement of fluorescence emission, improved fluorophore photostability, and significant reduction of fluorescence lifetime have been obtained from high aspect ratio Ag NWs. The samples were excited at different wavelengths and the respective emissions were recorded. A solvato-chromic red shifted emission band at different solvent composition was observed. The data showed that Ag emissions followed the relationship in Equation 3.

$$n\lambda_{excitation} = 2n\lambda_{emission} \quad (3)$$

This is a typical non-linear second order optical trend demonstrated by Ag NWs following the equation 3, which resulted due to the electric-dipole interaction with radiation of strong intensity [33].

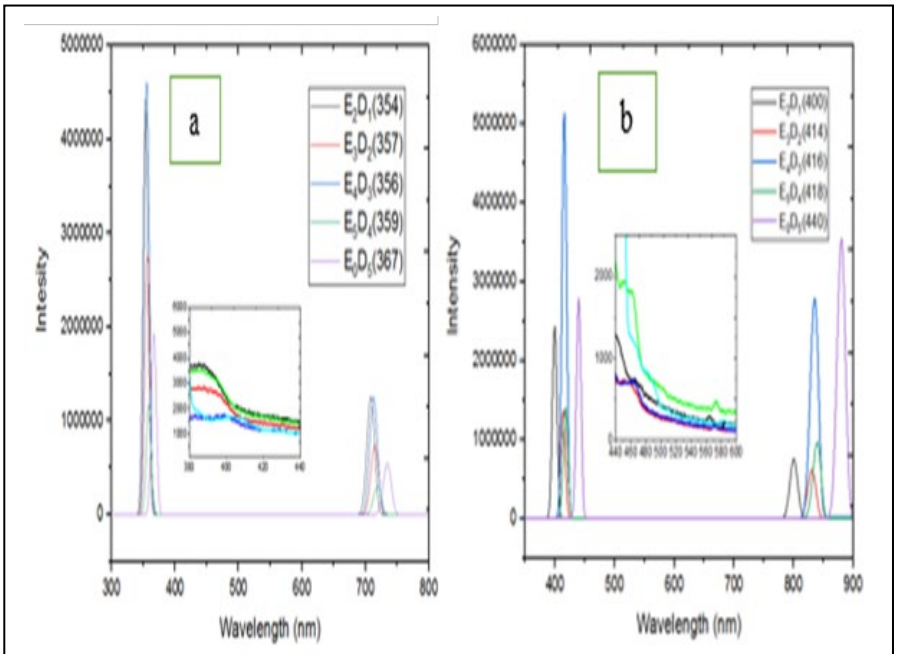

Figure 4. Photoluminescence spectra of Ag NWs at different excitation wavelengths from 354-440 nm for samples E_2D_1, E_3D_2, E_4D_3, E_5D_4, E_OD_5

3.6 DSC analysis

Thermal properties of samples were measured using differential scanning calorimetry (DSC) [34]. The amorphous domain of the Ag NWs were determined using a DSC heating rate of 10◦C/min and showed a large endothermic peak at 300 ºC as latent heat in Figure 5. Figure 5 (a, b, c) shows the DSC plots for samples E_2D_1, E_3D_2, E_4D_3, respectively. It is directly linked with the existence of amorphous domains or distorted crystal structures within each sample of Ag. The latent heat determined by DSC is possibly consumed by calcination or crystal reorganization. Such latent heat is greatly reflected by the samples which possess a higher extent of ultrathin Ag NWs. The E_4D_3 sample demonstrated a more intense peak compared to the others, where existence of small particles and ultrathin Ag NWs is also the dominant structure, as shown by SEM in Figure 1. It is further suggested by SEM that there is also the presence of cubic, hexagonal, rod like, rhombic, triangular and capsule shaped particles in the sample. These geometries have definite grain boundaries which are amorphous in nature, therefore such endothermal heat at latent temperature is explicitly assigned for these domains. Moreover, through the DSC analysis it can be concluded that the metal nanostructures which are usually estimated as highly crystalline in form, could possess the amorphous/grain boundaries or distorted crystal structures. The existence of such domains or structures are highly desired for the confinement of electrons and tuning conductivity. Therefore, the mixed solvent system could highly be a beneficial chemical approach where conduction of electrons at single electron level can be achieved via controlling the diameter scale and tailoring the amorphous domain.

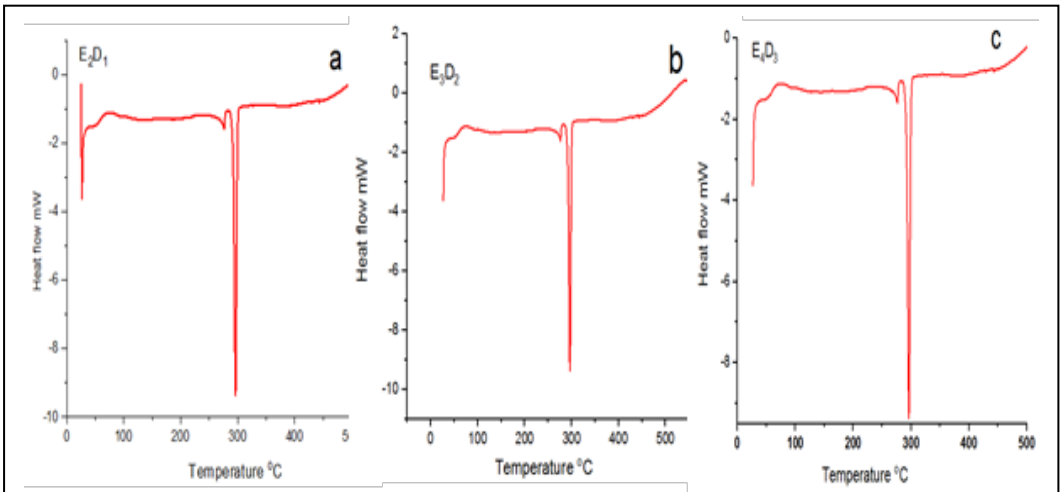

Figure 5. DSC curves of Ag NWs for samples E_2D_1, E_3D_2, E_4D_3

Conclusion

The mixed polyols synthesis process proved successful in the production of Ag NWs with a high aspect ratio. The data showed that this mixed polyol method resulted in the formation of ultrathin Ag NWs; and that the extent of DEG directly impacted the Ag NWs diameter. Moreover, the presence of Ag NPs including cubic, hexagonal, rod like, rhombic, triangular and capsule shaped was also observed. XRD characterization elaborated the materials as anisotropically crystalline mainly at phase (111) and phase distortions for extra thin diameters. Additionally, DSC highlighted the formation of significant grain boundaries, and these are more concentrated in the samples where ultrathin NWs are present and again where XRD phase distortion is seen. These findings supported the quantum confinement effect and trend of allowed electronic wave function (ψ) to tune their conductivity. Furthermore,

each sample had demonstrated SPR with λ_{max} in the range of 388 nm to 446 nm. The materials have also demonstrated second order optical trend for respective $\lambda_{max\ and}$ showed luminescence around 500 nm. These SPR and PL characteristics are highly desirable in the design of photovoltaic cells. Similarly, the existence of grain boundaries or amorphous domains mainly restrict electric conductivity, therefore these materials can find applications in the fabrication of diodes. Finally, ability to tune the formation of particle morphologies at specific DEG content, proved helpful in suggesting the mechanistic growth of Ag NWs.

Acknowledgments

The ORICMUST and HEC (Project Number:7183) Pakistan are gratefully acknowledged for the financial support to the study.

Conflict of Interest

The authors declare that they have no Conflict of Interest.

ORCID iDs

Sadia Sharif https://orcid.org/0000-0002-5960-1711

Zahoor Ahmad https://orcid.org/0000-0002-9076-9125

References

[1] Li, W.; Meredov, A.; Shamim, A, npj Flexible Electronics. **2019**, 3 (1), 1-7.

[2] Anh Dinh, D.; Nam Hui, K.; San Hui, K.; Singh, J.; Kumar, P.; Zhou, W., Rev. Adv. Sci. Eng. **2013,** 2 (4), 324-345.

[3] Cortes, L. Q.; Lonjon, A.; Dantras, E.; Lacabanne, C., **J**. Non- Cryst. Solids. **2014,** 391, 106-111.

[4] Jana, N. R.; Gearheart, L.; Murphy, C. J, Commun. Chem. **2001,** (7), 617-618.

[5] Gebeyehu, M. B.; Chala, T. F.; Chang, S.-Y.; Wu, C.-M.; Lee, J.-Y, RSC Adv. **2017,** 7 (26), 16139-16148.

[6] Zhu, J.-J.; Liao, X.-H.; Zhao, X.-N.; Chen, H.-Y., **Mater**. Lett. 2001, 49 (2), 91-95.

[7] Zahoor, A.; Teng, Q.; Wang, H.; Choudhry, M.; Li, X., Metals and Materials International.2011. 17 (3), 417-423.

[8] Ahmad, Z.; Maqsood, M.; Mehmood, M.; Ahmad, M. J.; Choudhary, M. A. Bulletin of Chemical Reaction Engineering & Catalysis. 2017, 12 (1), 127-135.

[9] Kaabipour, S.; Hemmati, S, Beilstein Journal of Nanotechnology 2021 12 (1), 102-136.

[10] Pulit-Prociak, J.; Banach, M., Open Chemistry 2016, 14 (1),76-91.

[11] Meshesha, B. T.; Barrabés, N.; Medina, F.; Sueiras, J. E.,

Nanotechnology, **2009**, 1, 87-91.

[12] Zhang, W.; Chen, P.; Gao, Q.; Zhang, Y.; Tang, Y., Chem. Mater. **2008**, 20 (5), 1699-1704.

[13] Wiley, B.; Sun, Y.; Xia, Y., Langmuir, **2005**, 21 (18), 8077-8080.

[14] Jia, C.; Yang, P.; Zhang, A., Mater. Chem. Phys. **2014**, 143 (2), 794-800.

[15] Yi, Z.; Xu, X.; Tan, X.; Liu, L.; Zhang, W.; Yi, Y.; Luo, J.; Yao, W.; Yi, Y.; Duan, T., Surf. Coat. Technol. **2017**, 327, 118-125.

[16] Chen, T.; Wang, H.; Yang, H.; Bai, S.; Guo, X., Mater. Res. Express, **2018**, 5 (6), 066426.

[17] Coskun, S.; Aksoy, B.; Unalan, H. E, Cryst. Growth Des. **2011,** 11 (11), 4963-4969.

[18] Sarkar, R.; Kumbhakar, P.; Mitra, A. K.; Ganeev, R. A., Curr. Appl. Phys. **2010**, 10 (3), 853-857.

[19] Araki, T.; Mandamparambil, R.; van Bragt, D. M. P.; Jiu, J.; Koga, H.; van den Brand, J.; Sekitani, T.; Den Toonder, J. M.; Suganuma, K., J. Nanotechnol. **2016**, 27 (45).

[20] Li, Y.; Yuan, X.; Yang, H.; Chao, Y.; Guo, S.; Wang, C., Materials. **2019,** 12 (3), 401.

[21] He, G.-C.; Lu, H.; Dong, X.-Z.; Zhang, Y.-L.; Liu, J.; Xie, C.-Q.; Zhao, Z.-S, RSC Adv. **2018,** 8 (44), 24893-24899.

[22] Zhang, P.; Wyman, I.; Hu, J.; Lin, S.; Zhong, Z.; Tu, Y.; Huang, Z.; Wei, Y., Mater. Sci. Eng. **2017**, 223, 1-23.

[23] Antarnusa, G.; Denny, Y. R.; Suherman, A.; Utami, I. S.; Saefullah, A, Chem. Eng. 2021, A**.** 14 (4), 335-346.

[24] Sun, Y.; Xia, Y., Advanced Materials, **2002**, 14 (11), 833-837.

[25] Kumar, H.; Rani, R., Int J Eng Innov Technol **2013,** 3 (3), 344- 348.

[26] Joya, K. S.; Ahmad, Z.; Joya, Y. F.; Garcia-Esparza, A. T.; Groot, H. J., Nanoscale, **2016,** 8 (32), 15033-15040.

[27] Ahmad, Z.; Choudhary, M.; Mirza, M.; Mirza, J., Mater Sci Poland, **2016**, 34 (1), 79-84.

[28] Yan, X.; Ma, J.; Xu, H.; Wang, C.; Liu, Y., J. Phys. D. **2016**, 49 (32), 325103.

[29] Chen, A.; Xie, H.; Wang, H.; Li, H.; Li, X., Synth. Met. **2006**, 156 (2-4), 346-350.

[30] Zhao, Y.; Fitzgerald, M. L.; Tao, Y.; Pan, Z.; Sauti, G.; Xu, D.; Xu, Y.-Q.; Li, D., Nano Letters **2020,** 20 (10), 7389-7396.

[31] Adhyapak, P.; Karandikar, P.; Vijayamohanan, K.; Athawale, A.; Chandwadkar, A., Mater. Lett. **2004**, 58 (7-8), 1168-1171.

[32] Korte, K. E.; Skrabalak, S. E.; Xia, Y., J. Mater. Chem. **2008**. 18 (4), 437-441.

[33] Prasad, P. N., Polym. J. 1991, 32 (10), 1746-1751.

[34] Zhang, L.; Zhu, W.; Huang, Y.; Qi, S: Synergetic effects of sil Zhang, L.; Zhu, W.; Huang, Y.; Qi, S.,

Nanomaterials, **2009**, 9 (9), 1264-1286.